JOURNAL OF THEORETICAL
AND APPLIED MECHANICS
43, 2, pp. 223-240, Warsaw 2005

MAGNETORHEOLOGICAL FLUID DAMPER WITH RADIALLY-SHAPED GAP AND CONTACT-LESS SEALING

BOGDAN SAPIŃSKI

Department of Process Control, University of Science and Technology, Cracow
e-mail: deep@agh.edu.pl

The paper is concerned with design, numerical study of magnetic fluid and experimental testing of a linear magnetorheological damper (MR damper) with radially-shaped gap and contact less sealing. Preferred embodiments for MR dampers development are outlined. The structure, materials used in the main components and operation principle of the damper are described. The magnetic field distribution in the damper in steady states and in transients is numerically studied. Force responses measured for the damper in the experimental setup are provided. Directions for further improvements are suggested.

Key words: magnetorheological damper, magnetic field, force response

1. Introduction

The actuation process in MR dampers converts the "driving energy" in the form of a magnetic field into "actuating energy" in the form of mechanical strain that allows us to modify the dynamic characteristic under varying conditions. MR dampers feature strongly non-linear dynamic characteristics. They are mostly a result of non-linearity introduced by the magnetic circuit consisting of ferromagnetic elements of the damper and a portion of the MR fluid affected by the magnetic field excited by the current in the coil. Hence, the processes in the MR fluid and the properties of coil circuit would determine the dynamic behaviour of the damper.

The functional relationship between the force (output), the piston velocity (input) and the magnetic field (control) is depicted in Fig. 1. The advantage of the MR damper is associated with the capability of continuous modification

of the damping characteristic throughout the controllable range. By applying real-time control schemes to the MR damper, vibration control can be achieved.

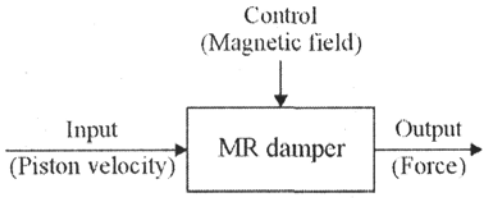

Fig. 1. Schematic diagram of an MR damper

Different MR damper constructions can be found in patent specifications and available literature e.g. (US Patent, 5,277,281, 1999; Bolter and Janocha, 1997; Lindler *et al.* 2000; Zhou and Zhang, 2002; Lord Corporation, 2003 etc.). In this paper, an experimental MR damper with radially-shaped gap and contact less sealing operating in the flow mode of the MR fluid is considered. The damper was designed and engineered basing on the patent specification (Sapiński and Szydło, 2002) and some results of the author's research program summarized in (Sapiński, 2004). The main objectives of the paper were: to present structure of the damper, to provide a better insight to the damper operation via numerical study of magnetic field distribution and to investigate experimentally force responses of the damper under the action of magnetic field.

2. Preferred embodiments of magnetorheological dampers

The relationship between size of the MR damper, displacement stroke (piston), control voltage level, MR fluid characteristics and the damper load can be appreciated from the general procedure of design of MR dampers described in (Bullough, 2000). The large number of variables to be taken into consideration in design and performance testing of MR dampers presents a difficulty in itself. This difficulty may be reduced by taking the simplification of a quasi-steady approach. The approach taken is to reduce parasitic friction as far as possible, to maximize controllability, while the design is considered in isolation from the compliance of other components; this is minimized in the performance testing with a stiff and high inertia test rig drive.

A simplified relationship for a fixed viscous damper is depicted in Fig. 2. For an assumed mass and suspension stiffness, the second order linear 1DOF

equation of motion leads to a fixed damping coefficient, where c denotes a constant of the proportion between the applied force and velocity of the suspended mass. The damping rate may be symmetrical or may have different (but fixed) values in compression or rebound of the suspension.

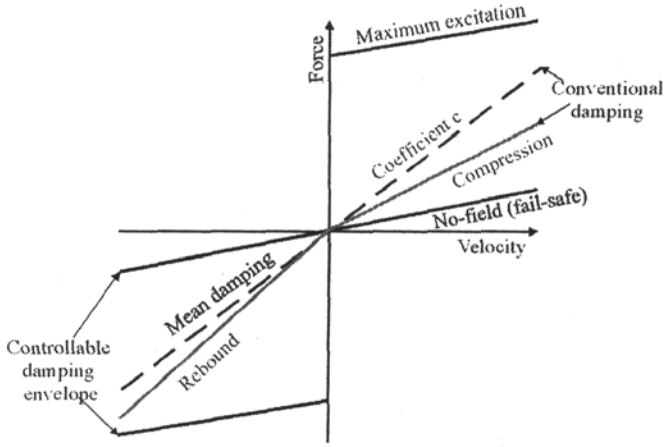

Fig. 2. Force vs. velocity curve and the envelope of a suspension damper: fixed viscous damper and MR damper

Figure 2 shows also the performance envelope of an MR damper. The minimum damping coefficient – a "fail-safe" condition – occurs under the conditions of zero excitation. Under magnetic field control and maximum excitation, the MR damper is capable of developing the maximum level of restoring force across the entire velocity range. The boundaries of zero excitation, maximum excitation, and maximum positive and negative velocity define a symmetrical envelope for the force-velocity-displacement map required of the MR damper, within and across which the MR damper will operate under control as demanded.

The major components of the MR damper, i.e. piston, control valve and cylinder, are determined by:

- envelope requirements of the operating conditions
- MR fluid characteristics
- maximum cylinder pressure
- available space for the complete MR damper, together with MR damper operating conditions and constructional considerations.

To maximize MR damper controllability, the effects of friction and fluid inertia, and compressibility have to be minimized. Summarizing, we conclude

that the MR damper operating envelope is defined in terms of the minimum damping (fail-safe) coefficient c, maximum piston force and velocity, and maximum cylinder pressure that is approximately the maximum MR control valve pressure drop.

3. Construction of the damper

The damper was intended for static and dynamic testing. On account of the experimental procedure, it might be required that the damper be assembled and refilled with an MR fluid in laboratory conditions. The damper disassembly must be easy, without damaging components, and the conditions for measurements have to be provided.

The damper was engineered with the following main design objectives: maximum axial force: 3000 N, maximum frequency: 10 Hz, maximum cylinder pressure: $2.5 \cdot 10^6$ Pa, maximum length (shaft is maximally protruded): 260 mm, maximum diameter: 55 mm, operating temperature: 70°C. The size of the damper must allow it to be mounted in a driver's seat in the experimental setup.

The structure of the damper and its major components are shown in Fig. 3. Cylindrical damper housing 1 is closed by covers 2 and 3. Upper cover 2 is sealed with an o-ring in the housing. Sealing ring 5 is fixed in the cover, to seal shaft 6. The lower damper section is sealed with ring 8, press-fitting membrane 9. This ring exerts pressure on the upper surface of diaphragm 9, right to the cut in the housing. The lower surface of the membrane is locked by lower cover 3. Dosing (cut-off) valve 14 is fixed in lower cover 3 to enable gas supply under pressure to the volume F between the membrane and the lower cover. The piston head assembly includes coil core 17 with windings 16 and insulation 15. The whole assembly, toroidal in shape and divided into six segments, is placed inside the coil housing and fixed with lower piston cover 18 and upper piston cover 19. The segments are secured in place by fastening plates 21 bolted to the coil core. The coil is supplied via wire 11 driven through a hole in the shaft. It is worthwhile to notice that there are two magnetic circuits in the damper: the main circuit closed by the fastening plates and the ancillary one closed by the housing. The main circuit controls the variations of damping characteristics. During piston movement, the MR fluid flows through radially-shaped gaps of the space beneath the piston to that above it or vice versa and hydraulic resistance is thus produced. Hydraulic resistance varies with MR fluid viscosity in the presence of magnetic field. The

main task of the ancillary circuit is to ensure effective piston sealing (between the piston head and the housing) thanks to higher viscosity of the MR fluid induced by permanent magnets 20 located on the piston head circumference between the upper and lower pole pieces.

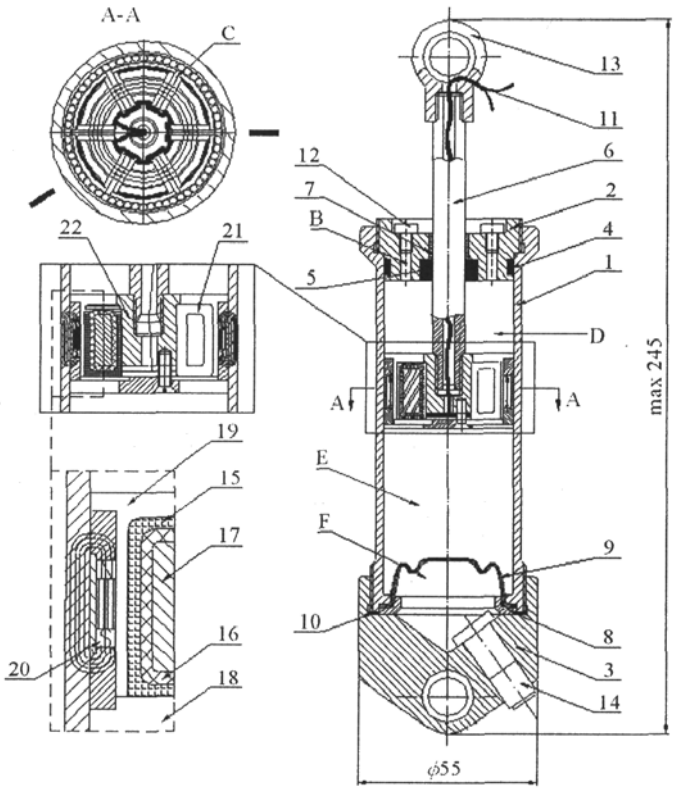

Fig. 3. Structure of the damper: 1 – housing, 2 – upper cover, 3 – lower cover, 4 – cover seal, 5 – shaft sealing, 6 – shaft, 7 – guiding element, 8 – pressing ring, 9 – diaphragm, 10 – ring-shaped sealing element, 11 – coil wire, 12 – threaded corks, 13 – shaft holder, 14 – dosing and cutting-off valve, 15 – coil electric insulation, 16 – coil, 17 – coil core, 18 – lower piston cover, 19 – upper piston cover, 20 – permanent magnet, 21 – fastening plate, 22 – coil housing, A-A piston cross-section, B – opening for MR fluid dosing, C – radial-shaped gap for MR fluid flow, D – space inside the damper on the shaft end, E – space inside the damper on the diaphragm side, F – space under the diaphragm

The coil core and pole pieces are made of a magnetic material (steel), while the coil housing and the cover are made of materials that do not display magnetic properties (i.e. have magnetic properties of the vacuum).

The coil windings are made of copper wire 20 mm in diameter. Each of the six segments had 105 windings. The permanent magnet assembly consists of 51 general-purpose permanent magnets. The measured resistance of the control circuit was 13.5 Ω. The damper is equipped with a hydraulic gas-filled accumulator. The compressed air at the pressure 1.2 MPa was supplied to the space beneath the diaphragm. The damper was filled up with 70 ml of the MR fluid.

Basic properties of the MR 132LD fluid used in the damper, specially intended for dampers, brakes and mounts (Lord Corporation, 2003) are: carrier fluid; synthetic oil, particles; iron, size: $\sim 3\mu$m, concentration by volume: 32%, concentration by weight: 80.74%, viscosity (is a function of shear rate): 0.94 Pa·s at $10\,\mathrm{s}^{-1}$ and 0.33 Pa·s at $80\,\mathrm{s}^{-1}$, density: $3.055\,\mathrm{g/cm}^3$, $\eta/\tau_y^2(H)$ (a parameter representing the ratio of viscosity and maximum shear stress squared): $6 \cdot 10^{-11}$ s/Pa, saturation of particles: 2.1 T, operating temperature: $(-40, +150)^\circ$C, time response; milliseconds (exact time response is dependent on a device).

The magnetisation characteristics, rheological characteristics and relationship between the viscosity and shear stress rate in *off* state (no magnetic field) are given in Fig. 4a,b,c, respectively.

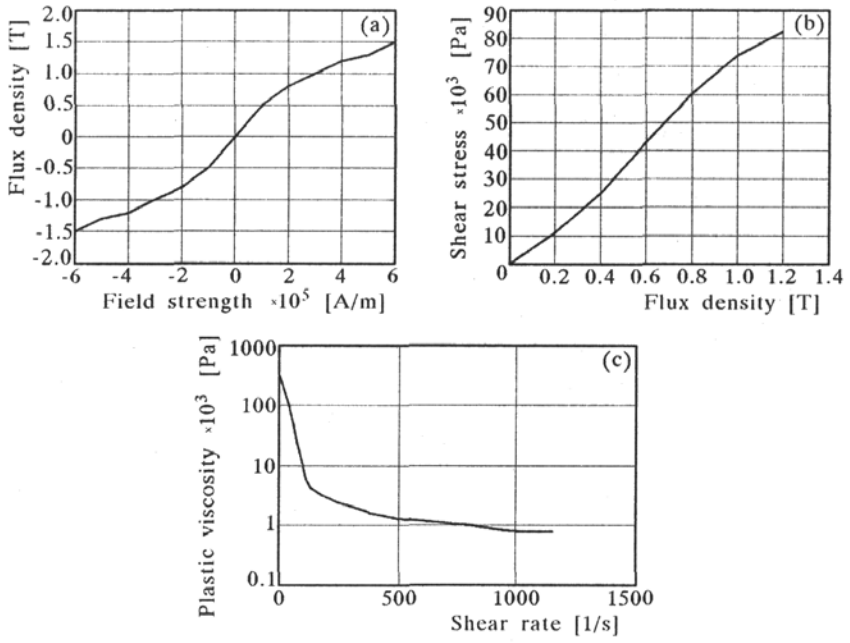

Fig. 4. (a) Flux density vs. field strength; (b) shear stress vs. flux density; (c) plastic viscosity vs. shear rate (no magnetic field)

Figure 5 shows a general view of the damper, Fig. 6a – piston head with pole pieces, Fig. 6b – piston head interior with coil segments and radial gaps and Fig. 6c – location of permanent magnets on the piston head circumference.

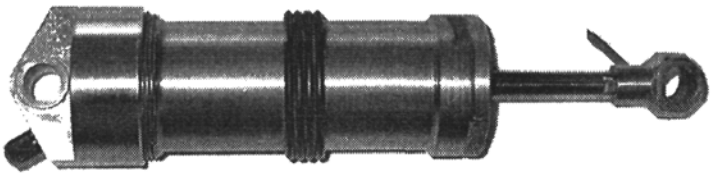

Fig. 5. General view of the damper

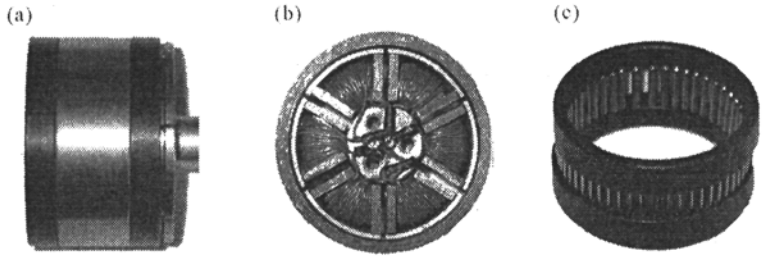

Fig. 6. (a) Piston head; (b) piston head interior; (c) location of magnets

4. Magnetic field in the damper

The knowledge of magnetic field in the MR damper is a vital problem for its performance. To provide a better insight in this field, we present results of computations performed to determine the magnetic field distribution in the damper, which proceeded its fabrication (Sapiński, 2004).

4.1. Field model of the damper magnetic circuit

It is assumed that materials from which the damper is made of are isotropic and the relationship between the magnetic field strength and induction for each material can be found from the relevant characteristics $B = f(H) = \mu(H)H$, where μ denotes magnetic permeability related to the field strength H. On account of the damper symmetry, a cylindrical-circular system of coordinates (r, φ, z) is introduced into mathematical description. The system of coordinates with a 3D image of the damper magnetic core is depicted in Fig. 7.

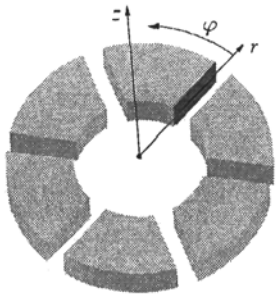

Fig. 7. The magnetic core image with the assumed coordinate system

To find the distribution of the magnetic field in the general case, Maxwell's equations (4.1) have to be solved with respect to the whole volume of the damper

$$\begin{aligned} &\operatorname{rot} \boldsymbol{E} = -\frac{\partial \boldsymbol{B}}{\partial t} \qquad && \operatorname{rot} \boldsymbol{H} = \boldsymbol{j} + \frac{\partial \boldsymbol{D}}{\partial t} \\ &\operatorname{div} \boldsymbol{B} = 0 && \operatorname{div} \boldsymbol{D} = 0 \end{aligned} \tag{4.1}$$

where: $\boldsymbol{E}$ – electric field strength, $\boldsymbol{D}$ – electric induction, $\boldsymbol{B}$ – magnetic flux density, $\boldsymbol{j}$ – surface density of current.

On account of the frequency of field variations in the gap, damper size and specificity of materials the damper is made of, the magnetic field ought to be treated as quasi-stable and the shift current and losses due to magnetic hysteresis can be ignored accordingly.

Introducing the vector potential $\boldsymbol{A}$

$$\boldsymbol{B} = \operatorname{rot} \boldsymbol{A} \tag{4.2}$$

and the magnetic field strength

$$\boldsymbol{H} = \frac{1}{\mu} \operatorname{rot} \boldsymbol{A} \tag{4.3}$$

equation $(4.1)_2$ can be rewritten as

$$\operatorname{rot} \left(\frac{1}{\mu} \operatorname{rot} \boldsymbol{A} \right) = \boldsymbol{j} \tag{4.4}$$

It is established that

$$\begin{aligned} &\operatorname{rot} \left(\frac{1}{\mu} \operatorname{rot} \boldsymbol{A} \right) = \frac{1}{\mu} \operatorname{rot} \operatorname{rot} \boldsymbol{A} - \operatorname{grad} \frac{1}{\mu} \times \operatorname{rot} \boldsymbol{A} \\ &\operatorname{rot} \operatorname{rot} \boldsymbol{A} = (\operatorname{grad} \operatorname{div} - \overline{\nabla}^2) \boldsymbol{A} \end{aligned} \tag{4.5}$$

and

$$\operatorname{div} \boldsymbol{A} = 0 \tag{4.6}$$

The magnetic permeability of homogeneous and isotropic media is a function of the absolute value of magnetic field strength: $\mu = \mu(|\boldsymbol{H}|)$, hence $\operatorname{grad}(1/\mu) = 0$ and then equation (4.4) can be rewritten as

$$\frac{1}{\mu}\overline{\nabla}^2 \boldsymbol{A} = -\boldsymbol{j} \tag{4.7}$$

where $\overline{\nabla}^2 \boldsymbol{A}$ denotes the Laplacian of the potential vector $\boldsymbol{A}$.

In the damper geometry considered here, the current density has two components only: j_r and j_z as the coil exciting the magnetic field is toroidal with a rectangular cross-section, hence

$$\boldsymbol{j} = j_r \mathbf{1}_r + j_z \mathbf{1}_z \tag{4.8}$$

The damper components occupy domains displaying certain properties:

- domain 1: coil with electric current; magnetic permeability equals that of vacuum $\mu = \mu_0$
- domain 2: dielectric piece insulating the coil; electric conductance $\gamma = 0$, no current flow, magnetic permeability $\mu = \mu_0$
- domain 3: MR fluid: electric conductance $\gamma = 0$; no current flow, the relationship $B(H)$ obtained from the magnetization curve
- domain 4: steel components; electric conductance γ, no current flow, the relationship $B(H)$ obtained from the magnetization curve.

The requirement given as equation (4.7) has to be satisfied in all the considered domains. Solutions obtained in domains 1-4 have to meet the following conditions:

- tangent components of the magnetic field strength have to be equal
- the vector potential function must be continuous on the boundary between the domains.

The magnetic field strength $\boldsymbol{H}$ is obtained from equation (4.3) on the basis of the computed value of the vector potential $\boldsymbol{A}$.

4.2. Field distribution in steady states

In steady states, the field analysed is magnetostatic, and the main objective is to obtain the distribution of magnetic flux density in the gap. In domains 1-4 occupied by damper components, the magnetostatic field is governed by the following equations of the vector potential $(\boldsymbol{A}_1, \boldsymbol{A}_2, \boldsymbol{A}_3, \boldsymbol{A}_4)$

$$\begin{aligned} \overline{\nabla}^2 \boldsymbol{A}_1 &= -\boldsymbol{j} & \overline{\nabla}^2 \boldsymbol{A}_2 &= \boldsymbol{0} \\ \overline{\nabla}^2 \boldsymbol{A}_3 &= \boldsymbol{0} & \overline{\nabla}^2 \boldsymbol{A}_4 &= \boldsymbol{0} \end{aligned} \tag{4.9}$$

The computation procedure uses values of magnetic parameters and geometrical dimensions of the damper components making up the magnetic circuit in the damper and the boundary conditions.

A simplified sketch of domains in which the field is calculated together with the field lines for a quarter of magnetic core is shown in Fig. 8.

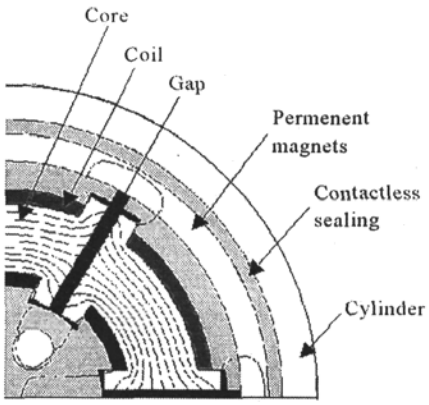

Fig. 8. Simplified sketch of a magnetic core quarter

As shown in Fig. 9, the planes $r\varphi$ and rz are considered in the investigations. The calculation procedure uses the FEM approach available in FLUX 3D (Cedrat, 2000). Computation results yielding magnetic field distributions are shown in Fig. 10 and Fig. 11.

Figs 10a,b show the flux density components $B_\varphi(r)$ for $\varphi = 0$, $z = 0$ and $B_z(r)$ for $\varphi = 0$, $z = 0$. Fig. 11a provides the flux density component $B_\varphi(z)$ for $r = 11.5 \cdot 10^{-3}$ m, $\varphi = 0$. Fig. 11b presents the flux density component $B_\varphi(r, z)$ for $\varphi = 0$. The grey areas in Fig. 10 correspond to damper components whose magnetic properties are those of vacuum.

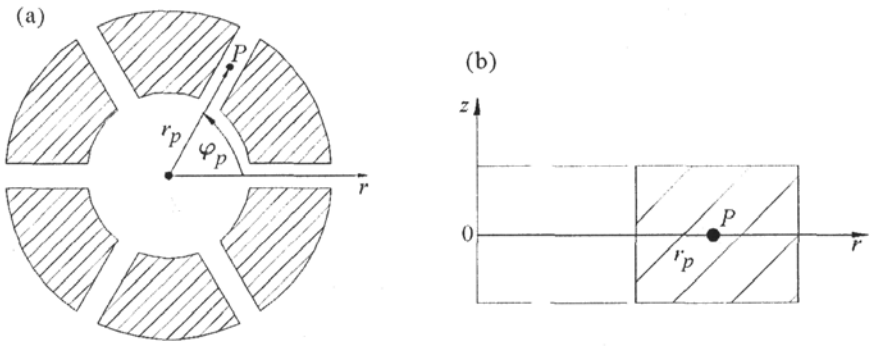

Fig. 9. Cross-section of the magnetic core: (a) plane $r\varphi$, $z = 0$; (b) plane rz, $\varphi = \varphi_p$

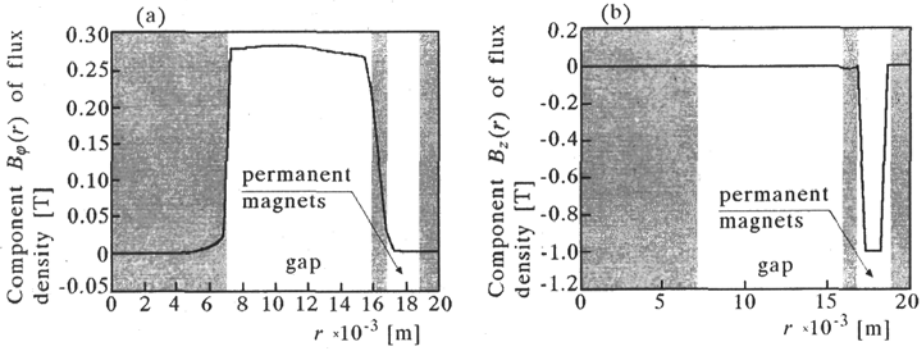

Fig. 10. The component $B_\varphi(r)$ (a) and $B_z(r)$ (b) of the flux density for $\varphi = 0$, $z = 0$

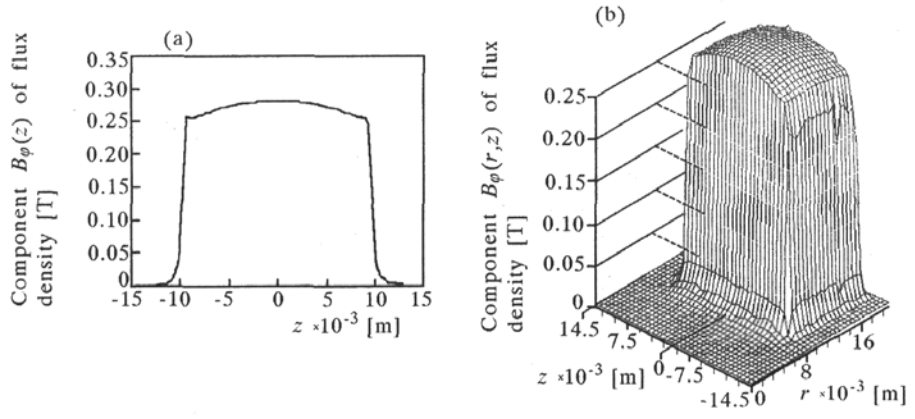

Fig. 11. The component $B_\varphi(r)$ of the flux density; (a) $r = 11.5 \cdot 10^{-3}$ m, $\varphi = 0$, (b) $\varphi = 0$

4.3. Field distribution in transients

The magnetic field in transients is governed by formulas

$$\operatorname{rot} \boldsymbol{E} = -\frac{\partial \boldsymbol{B}}{\partial t} \qquad \operatorname{rot} \boldsymbol{H} = \boldsymbol{j} \qquad \operatorname{div} \boldsymbol{B} = 0 \tag{4.10}$$

Introducing the vector potential in accordance with (4.4), yields

$$\overline{\nabla}^2 \boldsymbol{A} = -\mu \boldsymbol{j} \tag{4.11}$$

Accordingly, equation $(4.10)_1$ can be rewritten as

$$\operatorname{rot} \boldsymbol{E} = -\frac{\partial}{\partial t}(\operatorname{rot} \boldsymbol{A}) = -\operatorname{rot} \frac{\partial \boldsymbol{A}}{\partial t} \tag{4.12}$$

which yields the thus induced electric field strength

$$\boldsymbol{E}_i = -\frac{\partial \boldsymbol{A}}{\partial t} \tag{4.13}$$

In conducting materials, it is accompanied by the flow of current with the density

$$\boldsymbol{j}_i = \gamma \boldsymbol{E}_i \tag{4.14}$$

In steel components, there will be eddy currents with the density

$$\boldsymbol{j}_i = \gamma_{Fe} \boldsymbol{E}_i \tag{4.15}$$

In the domain occupied by the coil that induces the electromagnetic field, the current density is equal to

$$\boldsymbol{j}_{Cu} = \gamma_{Cu}(\boldsymbol{E}_i + \boldsymbol{E}_s) = (\boldsymbol{j}_i + \boldsymbol{j}_s) \tag{4.16}$$

Step-like voltage signals applied to the coil are considered in computations.

The electric field $\boldsymbol{E}_s$ is directly induced by voltage applied to the coil clamps. It is equal to the field produced in coil windings in steady states when constant excitations are applied

$$\boldsymbol{j}_s = j_r \mathbf{1}_r + j_z \mathbf{1}_z \tag{4.17}$$

The field $\boldsymbol{E}_i$ is induced in the coil windings due to time variations of the magnetic field (4.13) and constitutes a transient component of the electric field.

The equations of vector potential in the domains corresponding to damper components are written as

$$\begin{aligned} \overline{\nabla}^2 \boldsymbol{A}_1 &= \frac{\partial \boldsymbol{A}_1}{\partial t} - \mu_0 \boldsymbol{j}_s & \overline{\nabla}^2 \boldsymbol{A}_2 &= \boldsymbol{0} \\ \overline{\nabla}^2 \boldsymbol{A}_3 &= \boldsymbol{0} & \overline{\nabla}^2 \boldsymbol{A}_4 &= \mu(H)\gamma_{Fe}\frac{\partial \boldsymbol{A}_4}{\partial t} \end{aligned} \tag{4.18}$$

To obtain the distributions of magnetic field in the damper in transient states (when the voltage u is applied to the coil), equations (4.18) have to be solved. The results of computations are shown in Figs 10a,b. They provide time patterns of the component $B_\varphi(t)$ at the point P with the coordinates ($r = 11.5 \cdot 10^{-3}$ m, $\varphi = 0$, $z = 0$), (Fig. 12a) and of the current in the coil (Fig. 12b) for the step-like voltage $u(t) = A_0 \cdot 1(t)$ applied ($A_0 = 2$ V and $A_0 = 5$ V).

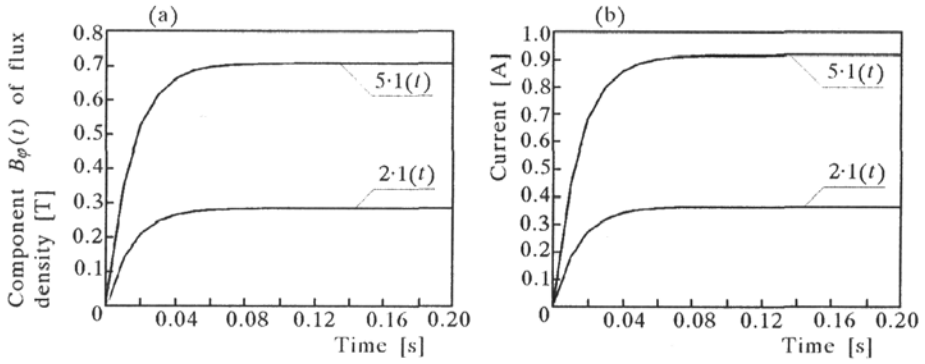

Fig. 12. (a) The component $B_\varphi(t)$ of the flux density vs. time in the point P ($r = 11.5 \cdot 10^{-3}$ m, $\varphi = 0$, $z = 0$); (b) current in the coil vs. time

5. Functional testing

The main aim of the testing program was to check the adequacy of the design objectives and compatibility of the damper components and subassemblies. In order to check that compatibility, the performance of the developed MR damper as a passive damper was tested. In introductory tests, we used the oil of Amortyzol 15 WL-150, intended for hydraulic shock-absorbers, due to high costs of the MR fluid. The oil in the amount of 70 ml was used in single damper filling. When the damper was filled with the oil, air compressed at

the pressure 1.2 MPa was supplied to the space beneath the diaphragm. The piston with the shaft is moved to the minimal position of the damper length, and at that pressure the shaft automatically protrudes. The thus prepared damper was tested in a vibrating testing machine to obtain force responses. In the course of further tests, the damper operation was checked for disturbances due to design errors, inappropriate assembly and wrong choice of sealing materials and components. Such disturbances were not observed.

In the next step, we checked the coil circuit of the damper. For this purpose, current responses in the coil to step-like and PWM (pulse width modulated) voltage inputs were measured. The obtained patterns of current in the coil did not display any disturbances.

Then the damper was disassembled and assembled again in accordance with the approved procedure (the damper was filled up with 70 ml of MR 132 LD fluid, and compressed air at the pressure 1.2 MPa was supplied to the space beneath the diaphragm). The thus prepared damper was examined in the experimental setup (see Subsection 5.1) in order to determine force responses under the action of magnetostatic fields in terms of the applied current, excitation frequency and amplitude.

5.1. Experimental setup

The experimental setup completed with the computer-controlled vibrating testing machine is schematically shown in Fig. 13a (Sapiński, 2003). On account of the limited clipping head of the vibrating machine, special fixtures were fabricated to allow the damper to be tested. The damper was placed and held in the machine in the extended position with fixtures (Fig. 13b). In the experiments, the piston was initially in the mid-stroke position.

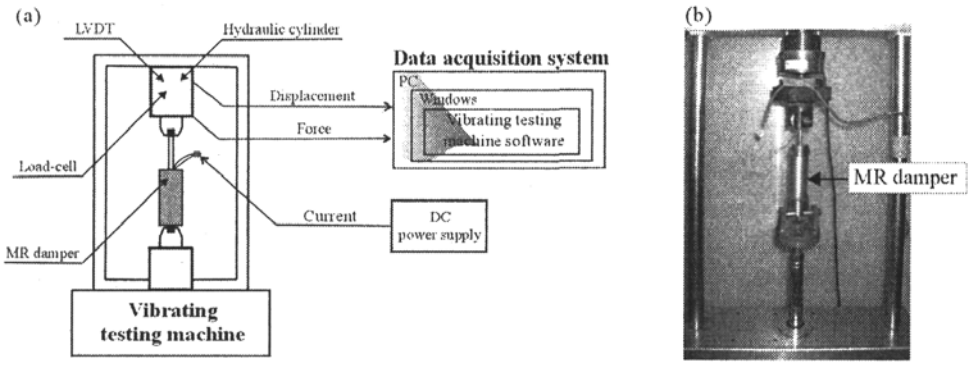

Fig. 13. (a) Schematic diagram of the experimental setup; (b) MR damper ready for tests

5.2. Force responses

The vibrating testing machine was programmed to 20 measurement cycles to generate a sine wave for three levels of frequency (1, 2.5, 4) Hz which correspond to amplitudes (10, 4, 1.5)·10^{-3} m. Force responses (force-time patterns, force-displacement curves and force-velocity curves) were evaluated for three levels of the applied current (0.00, 0.10, 0.20) A. The time history of piston velocity was computed basing on piston displacement. In Fig. 14 and Fig. 15, we present experimental data plots of force responses obtained under sine displacement excitations at the frequency 1 Hz (amplitude $10 \cdot 10^{-3}$ m) and 4 Hz (amplitude $1.5 \cdot 10^{-3}$ m). The plots were found on the basis of measurement data obtained in cycles 8-12.

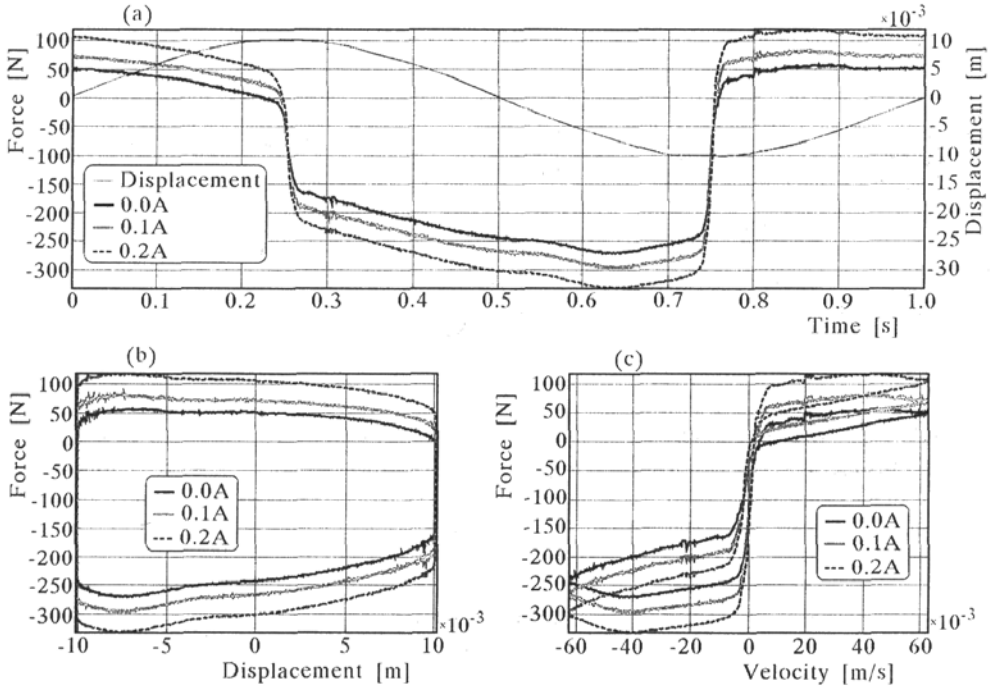

Fig. 14. Experimental data plots under the sine displacement excitation (frequency 1 Hz, amplitude $10 \cdot 10^{-3}$ m): (a) force-time patterns, (b) force-displacement loops, (c) force-velocity loops

The tests reveal that the influence of the applied current on the force response in the damper is only minor in the investigated range of (0.00, 0.20) A. That might be due to a small number of windings wound on coil core segments, which limits the field produced by the current in the coil, and hence the magnetic flux density in the gap. The reported non-symmetrical force vs.

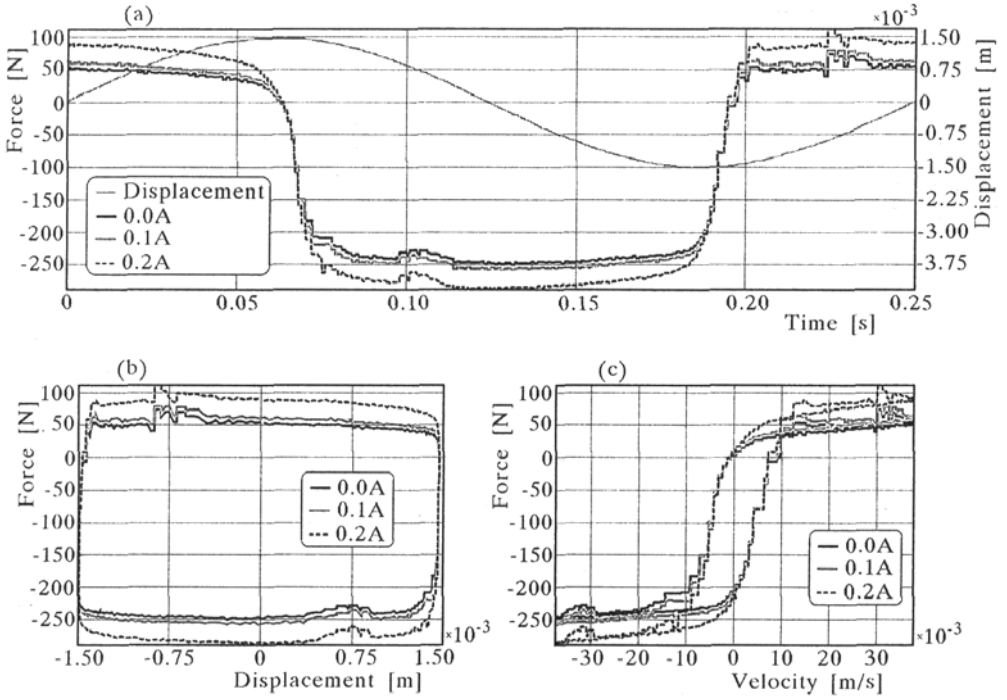

Fig. 15. Experimental data plots under the sine displacement excitation (frequency 4 Hz, amplitude $1.5 \cdot 10^{-3}$ m): (a) force-time patterns, (b) force-displacement loops, (c) force-velocity loops

time (displacement, velocity) relation imply an increase of the piston resistance during the compression phase and a decrease in the rebound phase.

6. Conclusions

The subject matter of the study was to present the development of an experimental MR damper with a radially-shaped gap and contact-less sealing. The design and structure of the damper were described. The magnetic field in the damper in steady states and in transients was numerically studied. Force responses (force-time patterns, force-displacement curves and force-velocity curves) under the action of magnetostatic fields were evaluated.

The computed distribution of magnetic flux density in the gap confirmed the adequacy of the adopted magnetic core piece design. The applied sealing between the piston head and damper cylindrical housing proves to be effective.

The obtained time patterns of magnetic flux density and current in the coil allowed complete analysis of damper behaviour as an actuator in a real-life application.

Preliminary tests of the damper in which force responses were investigated confirmed the design adequacy. The damper is now being thoroughly tested in the experimental setup over a wider range of piston velocities and current levels. Intensive research work on the developed damper is currently followed with an eye: to optimize electromagnetic circuits, to reduce piston friction resistance and to select the appropriate sealing, to select the gas filling the accumulator and adjust gas pressure.

This work was partially supported by the State Committee for Scientific Research as a part of the research project No. 5T07B 02422.

References

1. BOLTER R., JANOCHA H., 1997, Design rules for MR actuators in different working modes, *Proc. of SPIE*, **3045**, 148-159
2. BULLOUGH W.A., 2000, *Rheological Fluids, Advanced School on Smart Structures: Theory and Applications*, CISM, Italy 3
3. LINDLER J.E., DIMOCK G.A., WERELY N.M., 2000, Design of a magnetorheological automotive shock absorber, *Proc. of SPIE*, **3985**
4. SAPIŃSKI B., SZYDŁO Z., 2002, Tłokowy tłumik drgań liniowych, z cieczą magnetoreologiczną, Zgłoszenie projektu wynalazczego P-356512
5. SAPIŃSKI B., 2003, Dynamic characteristics of an experimental MR fluid damper, *Engineering Transactions*, **51**, 399-418
6. SAPIŃSKI B., 2004a, *Linear Magnetorheological Fluid Dampers for Vibration Mitigation: Modelling, Control and Experimental Testing*, Rozprawy Monografie AGH, **128**
7. SAPIŃSKI B., 2004b, Study of magnetic field in an experimental MR linear damper with radial-shaped gap and contact-less sealing, *Proc. of the Symposium on Smart Materials for Engineering and Biomedical Applications*, China, 137-145
8. ZHOU G.Y., ZHANG P.Q., 2002, Investigation of the dynamic mechanical behaviour of the doubled-barreled configuration in a magnetorheological fluid damper, *Smart Materials and Structures*, **11**, 230-239
9. CEDRAT, 2000, User's guide FLUX 3D, France

10. LORD CORPORATION, 2003, http://www.rheonetic.com

11. US PATENT, 5,277,281, 1999, Magnetorheological Fluid Dampers

Tłumik magnetoreologiczny ze szczeliną promieniową i bezstykowym uszczelnieniem tłoka

Streszczenie

W artykule przedstawiono projekt, analizę numeryczną pola magnetycznego oraz badania eksperymentalne liniowego tłumika magnetoreologicznego (MR) ze szczeliną promieniową i bezstykowym uszczelnieniem tłoka. Omówiono ogólne zalecenia do konstrukcji tłumików MR. Opisano budowę tłumika, scharakteryzowano materiały konstrukcyjne, z których wykonano jego główne elementy oraz opisano zasadę działania tłumika. Zamieszczono wyniki obliczeń numerycznych rozkładu pola magnetycznego w tłumiku w stanach ustalonych i nieustalonych. Przedstawiono wyniki pomiarów siły tłumienia na stanowisku badawczym. Sformułowano uwagi dotyczące udoskonalenia konstrukcji opracowanego tłumika.

Manuscript received November 12, 2004; accepted for print January 12, 2005